Experimental Comparison of Scroll and Swash-Plate Compressors for PV Driven Compression Chillers and Heat Pumps

Bernd Heithorst[1], Gregor Bauer[1], Benedikt Rauscher[1], Ludwig Irrgang[1], Markus Spinnler[1], Thomas Sattelmayer[1]

[1] Institute of Thermodynamics, Department of Mechanical Engineering, Technical University of Munich, Munich (Germany)

Abstract

A scroll and a swash-plate compressor are compared with each other, regarding their capability to operate in a PV-driven vapor cycle. Compressors for PV driven applications need a wide operation range and a dynamic control behavior. The comparison is performed in three steps: Firstly, the performance in steady-state operation, secondly, the controllability in dynamic operation and, thirdly, the operation under realistic boundary conditions. It is shown that the swash-plate compressor has a wider operation range with low part-load capability down to 18.9%. Regarding the controllability, the swash-plate compressor shows severe oscillations after a sudden decrease of the power signal. Finally, both compressor types are operated in a hardware in the loop simulation considering the generated PV power as well as electric and thermal demand of a single-family house in Munich to evaluate their applicability in PV driven applications.

Keywords: Solar Cooling, Solar Heating, PV, Scroll Compressor, Swash-Plate Compressor

1. Introduction

For small-scale solutions in solar cooling, photovoltaic (PV) plants coupled with compression chillers (CC) are more economic than ad- or absorption processes coupled with solar-thermal collectors (Lazzarin and Noro, 2018). Due to decreasing PV-panel prices, heat pumps (HP) coupled with PV become a more and more promising alternative for solar heating compared to fossil-fired boilers combined with solar-thermal collectors (Poppi et al., 2018, Tjaden et al., 2013).

If feed-in-tariffs are lower than the electricity prices, a high self-consumption ratio is required to achieve an economically reasonable system. This is especially important if the ratio between generated PV power and annual electricity demand is high (Luthander et al., 2015; Poppi et al., 2018). A HP or CC is one of the major electricity consumers in a building. Thus, the coupling between PV and HPs or CCs can lead to both, a high self-consumption and self-supply ratio.

Generally, state-of-the-art PV driven systems are equipped with a variable frequency drive (VFD) to ensure a flexible compressor operation to respond to fluctuating PV power. The main focus in research is currently on improving the control strategy of the HP or CC regarding the considered energy system (e.g., Fischer et al., 2017; Sichilalu et al., 2017; Tygessen and Karlsson, 2016). To the knowledge of the authors, there is no recent research to adapt the compressor, which is the main component of the vapor cycle, to the needs of a PV driven HP or CC. The requirements for a PV-driven vapor cycle are:

- High flexibility to respond to fluctuations in PV power and electricity demand.
- Wide operation range to make use of PV power generated in times of low solar irradiation (morning and evening hours).

Spinnler et al. (2014) introduced a system using a swash-plate compressor that is mainly used in the automotive industry instead of the usually applied scroll compressors in residential applications. The advantage of the swash-plate compressor is a lower part load capability of about 10 % of the maximum power. Furthermore, Spinnler et al. (2014) write that the power of swash-plate compressors can be adjusted by two degrees of freedom, namely varying the rotational speed and the cylinder stroke. In contrast to that, in common scroll compressors only the rotational speed can be varied to control the compressor power (Spinnler et al., 2014).

doi:10.18086/eurosun2018.04.06 Available at http://proceedings.ises.org

The aim of this paper is to compare both compressor types regarding the aforementioned needs of PV driven HPs or CCs. In the first step, the efficiency of both compressor types in steady state operation is compared with each other. Subsequently, the dynamics of both compressors are evaluated and finally both compressors are operated under realistic boundary conditions in a hardware in the loop (HIL) simulation.

2. Working Principle of the Compared Compressor Types

Both compressor types investigated in this study are displacement compressors. These compressors increase the refrigerant pressure by reducing the compression chamber's volume (ASHRAE, 2012). Compressors are also distinguished regarding their drive enclosure. In case of hermetic compressors, a gastight casing contains the motor and the compression unit. Semi-hermetic casings also contain both the motor and compressor but are accessible for later service or repair. Generally, semi-hermetic compressor designs are made in a bolted construction. In contrast, open compressors are driven by a shaft that is connected to an external motor. Thus, a gas-tight sealing is needed between shaft and compressor crankcase (ASHRAE, 2012).

2.1 Scroll Compressor

Scroll compressors are based on an orbiting compression mechanism (ASHRAE, 2012). They consist of two spiral-shaped scrolls. One scroll is fixed in the compressor casing while the other one rotates on an orbital path around the shaft center. Illustrations and a more profound description can be found in literature e.g. in ASHRAE (2012), p. 38.24 or Wang et al. (2000), p. 11.45. The gas pockets formed between the contact lines of the orbiting and the fixed scroll and their respective baseplates are sealed by lubricating oil. During the rotation, the contact lines move along the scroll flanks. Thus, the gas pockets are reduced in size and the refrigerant is compressed (Wang et al., 2000).

Different approaches are used to control the refrigeration capacity beside a trivial on/off control. A method that is frequently applied is *rapid-cycling*, where the distance between the two baseplates of the scroll is increased in times of thermal demand (e.g., Poort and Bullard, 2006). This basically results in a decreased volumetric efficiency of the compressor and thus is not favorable for an energy efficient capacity control. Another possibility is to adjust the rotational speed of the compressor. Here, the voltage and frequency of the alternating current (AC) of the motor are modified in a variable frequency drive. Then the capacity of the compressor is nearly proportional to the rotational speed (ASHRAE, 2012).

2.2 Swash-Plate Compressor

Swash-plate compressors are a subcategory of piston-compressors. They are mainly used in the automotive industry with the aim of generating a constant refrigerant volume flow at varying revolution numbers of the combustion motor (Stulgies et al., 2009). This is achieved through a variable cylinder stroke.

The cylinder stroke is adjusted by the inclination angle of the swash-plate. A sketch of an exemplary swash-plate geometry can be found e.g. in Tian et al. (2005). This inclination angle cannot be modified directly. It results from a force balance in the compressor's kinematics and depends on the rotational speed, the pressure on the suction and on the discharge side as well as on the pressure in the swash-plate chamber. The latter is adjusted by a mass flow compensation control valve that separates the swash-plate chamber from the discharge- and suction gas chamber (Tian et al., 2005). The valve is controlled with a voltage applied on the valve's coil U_{swash}. Thus, the voltage U_{swash} is the control variable of the compressor.

3. Methodology

In order to generate the required measurement results, both compressors are integrated in parallel in the same test rig. Thus, their performance can be compared under identical boundary conditions. To operate the compressors in a HIL-simulation, the test rig is embedded in a simulation environment. Both the test rig and the simulation environment are explained in more detail in the following.

3.1 Test Rig

Main Structure and Components

Figure 1 shows the hydraulic system sketch of the test rig. For the steady-state experiments, the installed swash-

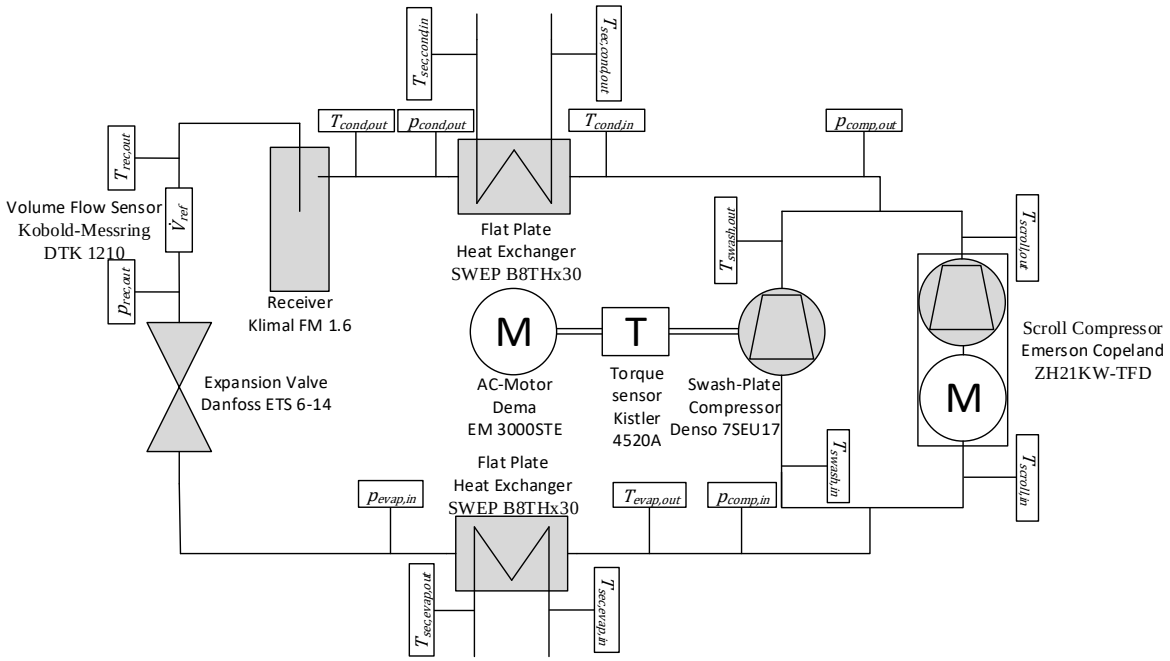

Fig. 1: Sketch of the test rig's hydraulics

plate compressor is a Denso 6SEU14 with 6 cylinders and a maximum displacement volume of 140 cm^3. For the dynamic experiments, a Denso 7SEU17 with a maximum displacement volume of 170 cm^3 and 7 cylinders was used. The swash-plate compressor is driven by an external air-cooled asynchronous motor. To calculate the mechanical power transferred to the compressor, a sensor for torque and rotational speed (Kistler 4520A) is installed between the AC-motor and the compressor. The installed scroll compressor is a hermetic Emerson Copeland ZH21KW-TFD with a displacement volume of 45 cm^3. Due to the hermetic design it is not possible to measure the mechanical power transferred to the scroll compressor. The AC-motors of both compressors are driven by a Danfoss VLT 3500 VFD with a maximum power of 3000 W. The main components are listed in table 1 in the appendix.

Condenser and evaporator consist of equal flat plate heat exchangers. The secondary circuit of the heat source is filled with a water-glycol mixture to allow operation below the freezing point. Water is used in the secondary circuit of the heat sink. For both heat exchangers, the mass flow rate and temperature of the incoming volume flow can be controlled. The accuracy of the temperature control is +/-0.5 K for the evaporator and +/- 0.3 K for the condenser in steady state operation.

Measurement Devices, Data Acquisition and Post Processing

As shown by figure 1, the test rig is equipped with different measurement devices. Table 2 in the appendix lists the different sensors and their measurement accuracy. To obtain the measured signals, the test rig is equipped with a National Instruments cFP-1808 data acquisition (DAQ) system. For process control and data processing, the digitalized signals are processed in a real-time MATLAB Simulink routine. The electric power consumed by the motors is measured in the VFD. The sample time of the power value is 1.3 s. The frequency of the generated AC-current is measured with a sample time of 0.29 s.

To obtain the performance data of the compressors in the test rig, it is necessary to calculate the specific enthalpy h, specific entropy s and the density ρ of the refrigerant using the measured state variables: pressure p and temperature T. For this purpose, the open source MATLAB plugin *CoolProp* (Bell et al., 2014) is used. Since the refrigerant volume flow rate $\dot{V}_{ref}$ is measured between the receiver and expansion valve, the mass flow is calculated with the density at the respective position:

$$\dot{m}_{ref} = \rho(T_{rec,out}, p_{rec,out}) \cdot \dot{V}_{ref} \qquad \text{(eq. 1)}$$

The obtained values for mass flow rate $\dot{m}_{ref}$ and specific enthalpy h are subsequently used to calculate the coefficient of performance (COP), the main parameter of the efficiency comparison of both compressor types.

Parameters for Performance Comparison

The performance of compressors is usually expressed in form of the COP. The COP is calculated using the capacity $\dot{Q}$ and the input power P of the compressor (ASHRAE, 2012):

$$COP = \frac{\dot{Q}}{P} \quad \text{(eq. 2)}$$

In heat pumps, the capacity $\dot{Q}$ is the condenser heat flow $\dot{Q}_{cond}$. The heat flow $\dot{Q}_{cond}$ for a system in steady-state can be calculated as follows:

$$COP = \frac{\dot{Q}_{cond}}{P} = \frac{\dot{m}_{ref}\left(h_{cond,in} - h_{cond,out}\right)}{P} \quad \text{(eq. 3)}$$

Here, $\dot{m}_{ref}$ is the refrigerant mass flow rate and $h_{cond,in}$ and $h_{cond,out}$ are the enthalpy at the condenser inlet and outlet, respectively.

In case of hermetic or semi-hermetic compressors, the input power P is the electrical power P_{el} of the motor, while the input power for open compressors is the mechanical power P_m of the driving shaft (ASHRAE, 2012). Since the drive enclosure of the considered scroll compressor is hermetic and the swash-plate compressor is an open-type, a common basis for the input power P of the COP-calculation is required. In preliminary experiments, it was found that the AC-motor of the swash plate compressor has a poor efficiency. This would cause an inappropriate disadvantage of the swash plate compressor when comparing the COP based on the electrical motor input power P_{el}. Using the mechanical power P_m of the compressor shaft is also not possible because the compressor shaft of the scroll compressor is not accessible. Therefore, the heat flow from the compressor into the refrigerant cycle $\dot{Q}_{comp}$ was chosen as the common basis. This heat flow can be calculated neglecting heat losses of the compressor crankcase to the ambient:

$$\dot{Q}_{comp} = \eta_{el} \cdot \eta_m \cdot P_{el} = \dot{m}_{ref} \cdot \left(h_{comp,out} - h_{comp,in}\right) \quad \text{(eq. 4)}$$

with the efficiency of the AC-motor, η_{el}, the mechanical efficiency of the compressor drive train and the compressor itself η_m, and the enthalpies at the compressor inlet $h_{comp,in}$ and outlet $h_{comp,out}$. The modified, thermal coefficient of performance, COP_{th}, can then be expressed as:

$$COP_{th} = \frac{\dot{Q}_{cond}}{\dot{Q}_{comp}} = \frac{h_{cond,in} - h_{cond,out}}{h_{comp,out} - h_{comp,in}} \quad \text{(eq. 5)}$$

Thus, the relation between the original COP and thermal COP is (again, neglecting heat losses of the compressor crankcase):

$$COP = \frac{COP_{th}}{\eta_{el} \cdot \eta_m} \quad \text{(eq. 6)}$$

The derived thermal COP is used to compare the efficiency of both compressors in the steady-state experiments.

3.2 Control for Dynamic Experiments

The HP or CC considered in this study is not intended to work in an off-grid system. Therefore, the system is not self-adjusting, and a control algorithm had to be designed that ensures that the compressor runs on the desired electric power. The designed controller consists of a PI-controller with integrated feed-forward control. A schematic diagram of the control system is depicted in figure 2. Li et al. (2009) and Lin et al. (2011) described similar approaches for controlling a variable speed compressor.

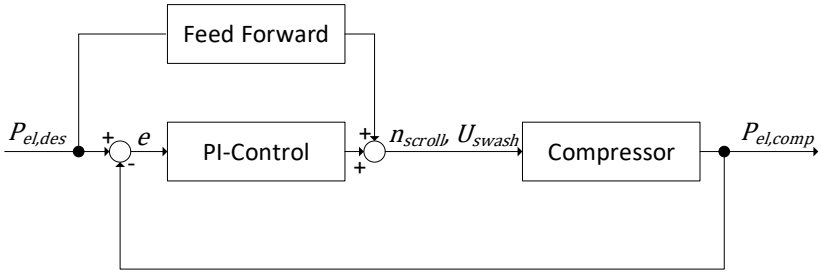

Fig. 2: Control system of the compressor

In this figure, the output value is the electric power consumption $P_{el,comp}$ of the AC-motor driving the compressor. The input value is the desired electric power consumption $P_{el,des}$. The control variables of the system for the two compressors differ: for the scroll compressor the control variable is the rotational speed of the compressor shaft n_{scroll}. The swash-plate compressor has two control variables: the rotational speed n_{swash} and the control voltage for the cylinder stroke U_{swash}, as explained in chapter 2.2. The control voltage U_{swash} is the main control variable, as it is shown in section 4.1 and is determined in the control scheme as described above. The rotational speed n_{swash} is controlled with the aim to run the motor at the lowest possible speed above the breakdown torque.

The principle idea of feed-forward controls is to measure disturbances and act before the disturbance interacts with the system (Seborg et al., 2010). The feed-forward control contains an inverse model of the process. Thus, the output of the feed-forward is an estimate for the control variable corresponding to the system's state based on the inverse model. The task of the PI-controller is finally to correct the error between the real system and the model incorporated in the feed-forward control.

3.3 Hardware in the Loop Simulation

In order to operate the compressor under realistic boundary conditions, the test-rig is embedded in a HIL-simulation. For the present study, it was decided to operate the vapor cycle as a heat-pump under mid-European boundary conditions. The elements of the HIL-simulation are depicted in figure 3.

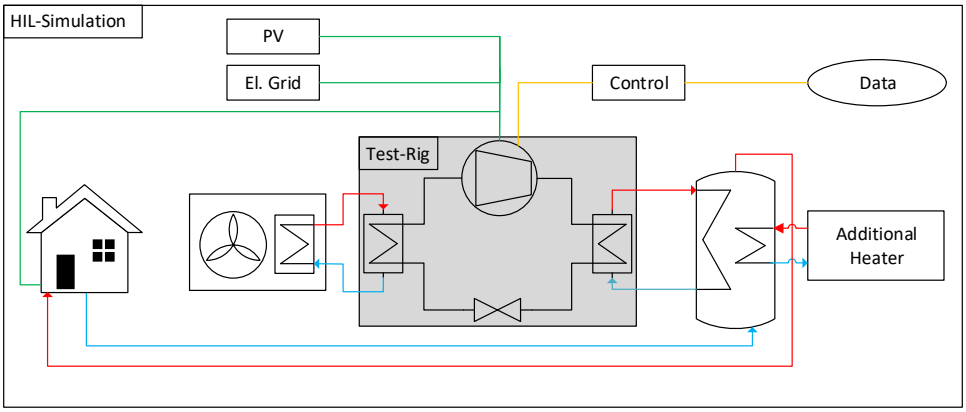

Fig. 3: Scheme of the considered system for the hardware in the loop simulation

It takes into account the thermal and electrical demand of a single-family house, the PV plant, the space heating and domestic hot water demand. This system consists of the heat pump, implemented in the test rig, a thermal storage, an additional ohmic heater to cover peak loads on cold winter days and a brine / air heat exchanger, serving as a heat source. The interfaces between the test rig (marked in gray) and the HIL-simulation are the liquid-inputs for condenser and evaporator. The temperature of the water entering the condenser $T_{sec,cond,in}$ is controlled to the simulated thermal storage temperature. Regarding the heat source, the temperature of the brine entering the evaporator $T_{sec,evap,in}$ is controlled to the ambient air temperature. In both, the heat exchanger with the ambient air and the heat exchanger inside the thermal storage, a temperature difference of 3 K is assumed between the fluid output temperature and the storage medium temperature or the ambient air temperature.

In order to resolve the dynamics in PV power generation and the electrical user demand, a fine resolution of the simulation and the necessary input data are required. In the following, the single elements are described in more detail:

- *PV plant*: For the PV plant measurements with a high temporal resolution of 1 s provided by *Solarenergieförderverein Bayern e.V.* are used to resolve the transient behavior of the PV power generation. The plant located in Munich is inclined at an angle of 28° in southern direction and has a capacity of 1 MW_p. For this study, the power was scaled to a size of 5 kW_p. The error in scaling a large-scale plant to the size of a typical single-family house rooftop plant was accepted because of the beneficial temporal data-resolution.
- *Electrical demand*: To consider the electric demand of the building's inhabitants without the demand of the heat pump, the data of HTW-Berlin (Tjaden et al., 2015) is used. The resolution of the electrical load-profile is 1 s.

- *Thermal demand*: The thermal demand of the 122 m² single family house with an annual energy demand of 40 kWh/(m² a) is modeled with the Building-Simulation-Tool introduced in a previous study (Heithorst et al., 2016). For this study, a day in November (Nov, 01th 2008) was chosen since it shows significant solar irradiation and relatively low environmental temperatures. Temperature and solar irradiation of the dataset of *Solarenergieförderverein Bayern e.V.* were used as well. The thermal energy demand for space heating during this day was 33.9 kWh.
- *Domestic hot water demand*: The energy demand for the domestic hot water supply was modeled with the tool *DHWcalc* (Jordan et al., 2017). As hot water demand and generation are decoupled by the thermal storage, a high temporal resolution is not as crucial as for the electricity demand.
- *Thermal storage*: The thermal storage is modelled as an ideally stirred vessel by a simple exergy balance since more advanced models e.g. for stratified storages showed problems in the real-time operation required for a HIL simulation. The volume of the storage is 400 l.
- *Control*: The system control calculates a desired compressor power $P_{el,des}$ to completely use the generated PV power P_{PV} in the building. In this study a basic rule-based approach is used to determine the power the compressor should utilize. It is based on two restrictions:

  1. *Thermal storage temperature:* If the thermal storage temperature exceeds the upper limit of 60°C, the compressor is shut off. If the temperature falls below a value of 38°C, the compressor is operated at $P_{el,des} = 2500$ W to ensure that the system covers the thermal demand of the building and domestic hot water.
  2. *Available PV power:* If the storage temperature is between the aforementioned limits, the compressor is operated with the PV power that remains after covering the electric demand of the inhabitants:

$$P_{el,des} = \begin{cases} P_{PV} - P_{Dem}, & if\ P_{PV} - P_{Dem} > 0 \\ 0, & if\ P_{PV} - P_{Dem} \leq 0 \end{cases} \quad \text{(eq. 7)}$$

4. Results & Discussion

4.1 Steady State Results

In total, 201 experiments with the swash-plate and 105 experiments with the scroll compressor were conducted in steady-state. The state of the experiment was assumed to be steady when variations in the heat sink temperature were below +/- 0.3 K, variations in the heat source temperature below +/- 0.5 K and the hot gas discharge temperature reached a steady level. Subsequently, a time series of 5 minutes was tracked. Finally, the measured and calculated state variables were averaged over the tracked time series and postprocessed.

Figure 4 shows the relation between the control variables of the swash plate compressor: the rotational speed n of the compressor shaft and the voltage U_{swash} applied to the pressure control valve.

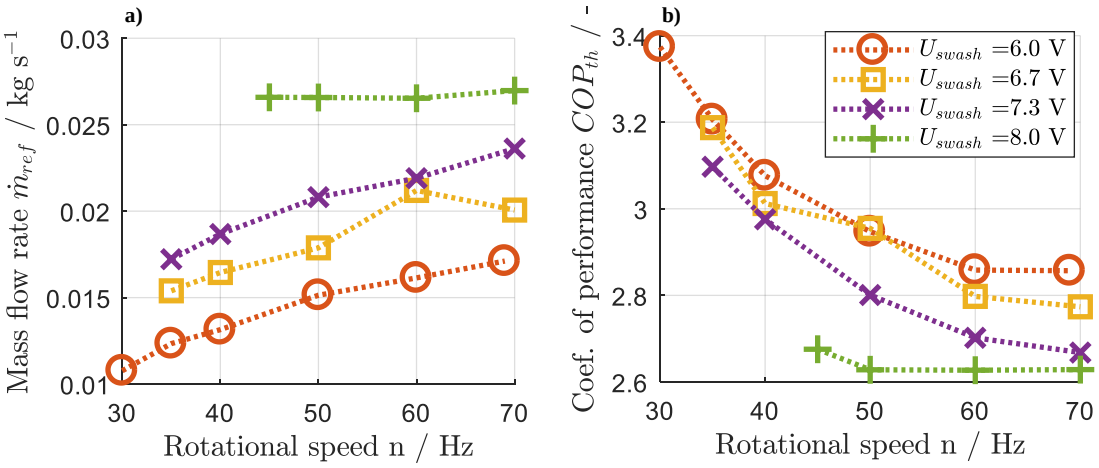

Fig. 4: a) Mass flow rate over rotational speed and b) thermal COP over rotational speed for swash-plate compressor experiments with a heat source temperature of 10°C and a heat sink temperature of 55°C

It can be seen in figure 4a) that a rise in the rotational speed n only leads to slight changes in the measured mass

flow rate and thus in the compressor's capacity. In the range of high compressor powers, the capacity is nearly constant. In contrast, the valve voltage U_{swash} shows a larger influence on the compressor capacity. The reason for this behavior is the original automotive application, where the aim is to minimize the influence of the variing rotational speed of the combustion motor on compressor capacity and thus on passenger comfort.

If the rotational speed n_{swash} is increased at a constant valve voltage U_{swash}, the force balance on the swash-plate is modified leading to a smaller displacement volume. Therefore, the dead volume at the top dead center of the compression rises and thus the efficiency of compression is reduced. Additionally, the friction losses inside the compressor rise at increasing rotational speed. The combination of both effects lead to a decrease of the thermal COP for increasing rotational speed, shown in figure 4b). Therefore, it is favorable to operate the swash-plate compressor at the lowest possible rotational speed. The AC-motor reaches its breakdown-torque if it is operated at low rotational speed and high loads. Therefore, it was decided to operate it at a fixed-speed $n_{swash} = 50$ Hz and variable valve voltage U_{swash} in the following steady-state experiments to be able to operate the compressor over the complete power range.

Figure 5 shows the performance comparison of the two compressor types.

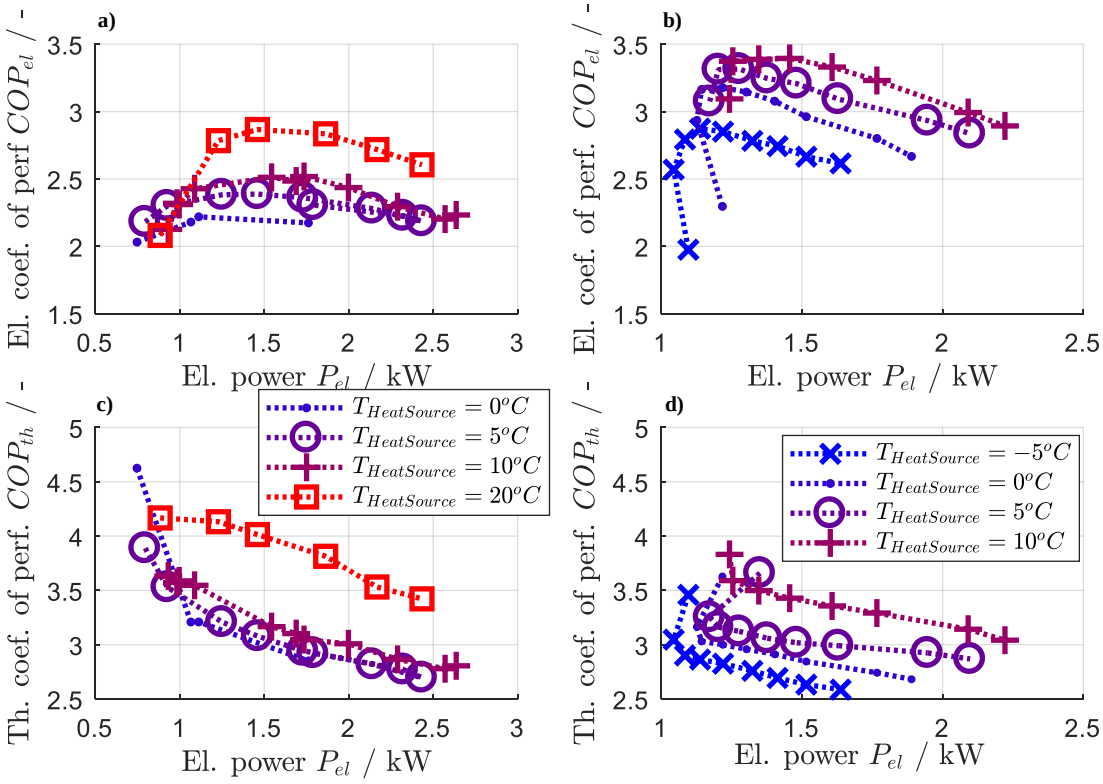

Fig. 5: COP based on electrical power of a) the swash-plate compressor and b) the scroll compressor. COP based on heat flow from c) the swash-plate compressor and d) the scroll compressor over the electrical motor power for steady-state experiments with a heat sink temperature of 45 °C

The figures 5a) and 5b) show the COP based on the electrical power for the swash-plate compressor (figure 5a)) and the scroll compressor (figure 5b)). Here, the inferior quality of the swash-plate compressor's AC motor becomes visible. In the figure 5b), a sharp decrease in the COP at low electrical powers P_{el} can be seen. Here, the AC-motor of the compressor advances towards its breakdown-torque. This leads to increasing electrical power consumption and decreasing mechanical power output. Thus, the operation in this regime should be avoided, also to prevent damages of the AC-motor.

The thermal COP based on equation 5 is shown in figure 5c) for the swash-plate compressor and in figure 5d) for the scroll compressor. Both compressors show a decreasing thermal COP with rising loads due to increasing friction losses. This effect is more prominent for the swash plate compressor. Additionally, the maximum electric power decreases with decreasing heat source temperature. In this regime, the maximum power of the scroll compressor is limited by the maximum allowable discharge gas temperature. The swash-plate compressor, in

contrast, is limited by the low suction pressure, as the control valve is adjusted to work at higher heat source temperatures due to the original application in automotive air conditioning. All in all, the thermal COP of the scroll compressor is slightly higher than for the swash-plate compressor for identical operation conditions.

It is also visible that the minimal electrical power of the swash-plate compressor is much lower than for the scroll compressor which is limited by the motor's breakdown-torque. The minimum part load values achieved are listed in table 1 for all combinations of heat source and heat sink temperatures.

Tab. 1: Minimum part load values determined for combinations of heat sink and heat source temperatures

		Swash-Plate				Scroll			
$T_{Heat\ Source}$ / °C		**0**	**5**	**10**	**20**	**-5**	**0**	**5**	**10**
$T_{Heat\ Sink}$ / °C	**35**	54.7	36.7	43.1	20.4	52.7	50.7	50.9	49.4
	45	42.4	28.9	25.7	18.9	63.8	59.6	55.9	55.95
	55	55.9	24.5	31.2	26.8	69.1	52.5	57.2	30.1

Table 4 shows that the minimum part load of the scroll compressor is always higher than 50% with an exception for the combination of a heat sink temperature of 55°C and a heat source temperature of 10°C. As the maximum power of the swash-plate compressor strongly depends on the heat source temperature and the minimum electric power is relatively constant (cf. figure 5a), the minimum operation range is wider for higher heat source temperatures. Due to the relatively high idle power of the swash-plate compressor, the minimum part load measured in the experiments is 18.9%. This is higher than the 10% expected by Spinnler et al. 2014, but it is obvious that the operation range of the swash-plate compressor can be much wider compared to the scroll compressor if the maximum power is not limited due to low heat source temperatures.

4.2 Results of Dynamic Operation

Different experiments were performed to evaluate the dynamic behavior of the two compared compressor types. The response of different controller types to a square wave signal with an amplitude of 1000 W and a step length of 10 s is demonstrated in more detail. As shown in figure 6, the DAQ-system leads to a delay between the rising or falling edges of the signal and the system response. The dead time of the DAQ-system was determined to be 375 ms.

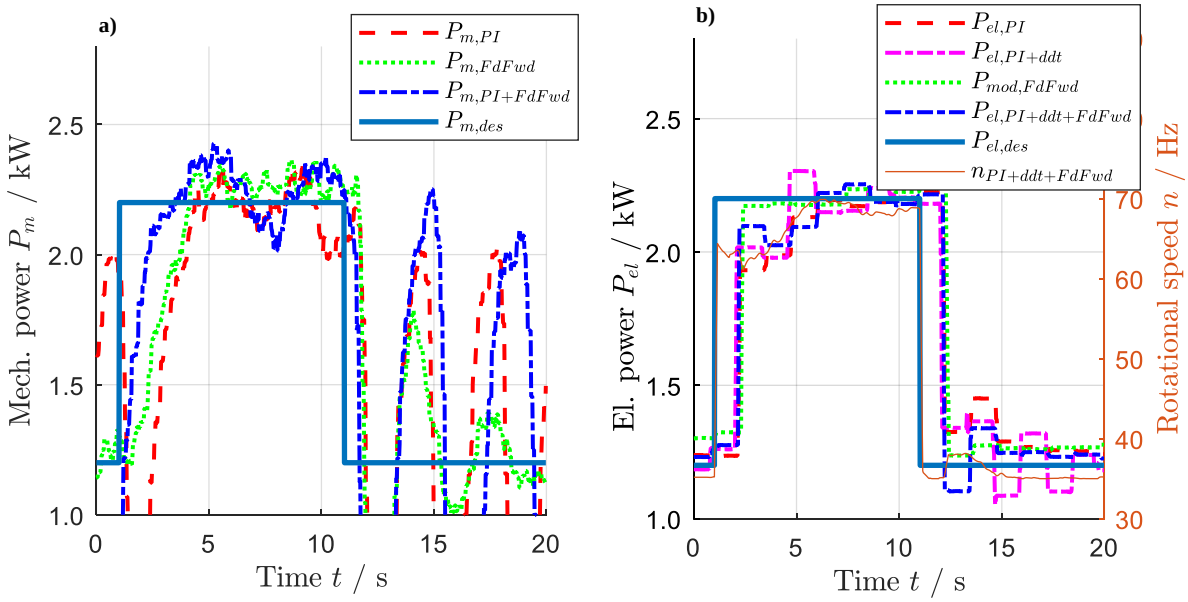

Fig. 6: Response of the compressors to a square wave signal with sample time 10 s and amplitude of 1000 W. a) swash-plate compressor: mechanical power over time b) scroll compressor: electrical power over time

The plot of the scroll compressor in figure 6b) shows a coarse temporal resolution of the electrical power P_{el} due

to the low temporal resolution of the power signal output at the VFD. Therefore, the rotational speed n of the compressor is depicted on the right y-axis as it has a better temporal resolution and proves that the signal does not show strong oscillations. Thus, even a simple control architecture using a PI-controller (red line) leads to good results showing only a small damping impact on the square wave signal. A controller using only the feed-forward control without an PI controller (green line) shows the fastest response on the rising edge, but also a constant offset after the downward edge because of the imperfections of the incorporated model. To avoid this offset, both controllers are coupled and a dead time compensation (ddt) is added. This combined controller (blue dash-dotted line) shows satisfactory results and is slightly damping the target signal with a settling time of 4.5 s.

In contrast to the scroll compressor, the swash-plate compressor, depicted in figure 6a) shows severe oscillations following on the falling signal edge for all considered control architectures. This oscillating behavior is caused by the complex control mechanism, where the power controller, the pressure controlling valve and the complex kinematics of the driving shaft, the swash-plate and the reciprocating cylinders interact. The response using only the feed-forward control shows the best damping behavior after the downward step. Therefore, the integral term of the PI-controller was made dependent on the valve voltage U_{swash}. For $U_{swash} < 5.5\ V$ K_I is set to 0. As it is shown later in the results of the HIL-simulation (figure 7), this improves the compressor control. However, complete damping could not be achieved.

From a dynamics point of view, the scroll compressor is more advantageous for a PV driven HP or CC, especially if the strong dynamics of an electric load profile must be taken into account.

4.3 Results of the Hardware in the Loop Simulation

Figure 7 shows the result of the HIL-simulation. Figure 7a) shows the desired power $P_{el,des}$ of the control (brown line). Especially at about 11:30 am the transient behavior of the electrical demand due to high load changes is visible. At the beginning of the day, the target power signal $P_{el,des}$ rises to a value of 2500 W when the storage temperature falls below the minimum limit (c.f. figure 7b)).

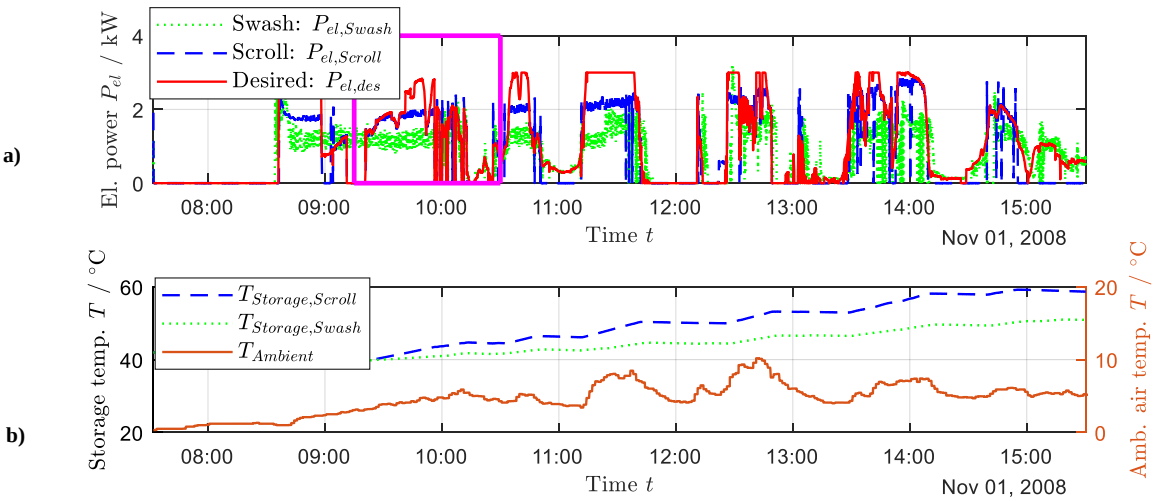

Fig. 7: Results of the HIL-simulation. a) desired and actual power of scroll and swash-plate compressor over time. b) thermal storage temperature development for scroll and swash-plate compressor operation and ambient temperature over time

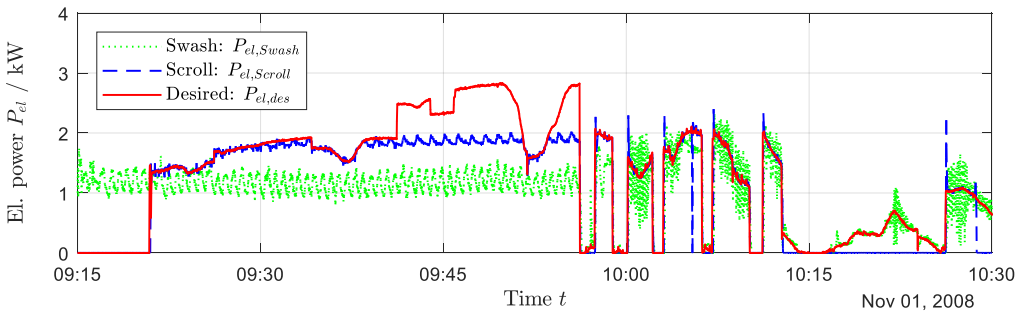

Fig. 8: Detail of figure 7a) (area marked in red) desired and actual power of scroll and swash-plate compressor over time

The swash-plate compressor (green line) shows the oscillations known from the square wave experiments. Furthermore, especially in the morning, it does not reach the required power due to the low outside temperatures which are between 3°C and 10°C, as it was also observed in the steady-state experiments in section 4.1. This problem is also visible but less dominant for the scroll compressor (blue line).

The advantage of the wide operation range of the swash-plate compressor is visible in figure 7a), e.g., at 14:30 hrs or between 10:15 hrs and 10:30 hrs (see additionally figure 8). While the scroll compressor must be switched off because the target power $P_{el,des}$ is lower than the minimum operation power, the swash-plate compressor continues working. Figure 8 shows the reduction of the compressor oscillations following a falling edge achieved by the adjustment of the integral gain K_I of the PI controller. However, at higher operation powers the oscillations are prevalent.

Furthermore, figure 8 shows, beginning at 09:55 hrs, that both compressor types follow the step gradients induced through the electric demand. It is visible that the scroll compressor follows the target signal accurately, when it is in its operation range. In contrast, the swash-plate compressor shows an oscillating behavior especially at higher electrical powers, but it is qualitatively following the target power signal.

To overcome the limited capacity of both compressor types at low ambient temperatures, a second shorter experiment between 11 am and 3 pm of the same day was conducted at fixed heat source and heat sink temperatures of 10°C and 50°C, respectively. Here, both compressors achieved the maximum capacity. The resulting self-consumption ratio of this experiment can be found in table 2:

Table 2: Comparison of the self-consumption ratio of experiment without HP, with scroll-compressor and with swash-plate compressor driven HP

Compressor	Only El. Demand	El. Demand + Scroll	El. Demand + Swash
Self-consumption ratio	31.5 %	85.1 %	91.4 %

Table 2 shows, that the self-consumption ratio rises about 53.5 % if a common variable speed HP is used. The implementation of a swash-plate compressor leads to an improvement of 6.3 % regarding the self-consumption ratio compared to the scroll compressor.

5. Conclusion

In the present study, a swash-plate and a scroll compressor were compared with each other regarding their applicability in PV driven heat pumps. In the steady-state experiments the scroll compressor showed a slightly better thermal COP but has a limited part load capability. The operation range of the swash-plate compressor is much wider (minimum part load 18.9 %). Regarding the dynamic experiments the swash-plate compressor showed severe oscillations of the compressor power after a sudden decrease in the desired power signal. In contrast, the scroll compressor showed a satisfactory control behavior. Finally, both compressors were operated under realistic boundary conditions in a HIL-simulation with a duration of one day. Despite its limited part-load capability, the scroll compressor used the generated PV power more efficiently than the swash-plate compressor. This is caused by the limited maximum power of the swash-plate compressor and its oscillating operation in the present control mode. If both compressors work in a regime where they can reach their maximum capacity, the swash-plate compressor shows an improvement of 6.1 % regarding the self-consumption ratio compared to the scroll compressor.

In conclusion, the presented study showed that the swash-plate compressor is difficult to control in a PV driven HP or CC. A possible solution to achieve both, a higher self-consumption ratio and a good controllability, could be an adapted scroll compressor with a reduced part load capability.

6. Acknowledgements

The project is funded by the Qatar National Research Funds (QNRF) under NPRP Funds Project #NPRP8-1908-2-760 and conducted in collaboration with the Qatar Environment and Energy Institute (QEERI). The authors thank *Solarenergieförderverein Bayern e.V.* for providing the PV-data.

7. Nomenclature

Quantity	Symbol	Unit
Coefficient of performance	*COP*	
Specific enthalpy	h	J kg^{-1}
Mass flow rate	$\dot{m}$	kg s^{-1}
Rotational speed	n	Hz
Pressure	p	Pa
Power	P	W
Heat flow	$\dot{Q}$	W
Temperature	T	K
Voltage	U	V
Volume flow rate	$\dot{V}$	m^3 s^{-1}
Efficiency	η	
Density	ρ	kg m^{-3}

Index	Meaning
comp	Compressor
cond	Condenser
Dem	Demand
des	Desired
ddt	Dead time compensation
el	Electric
FdFwd	Feed-forward
gen	Generated
in	Inlet /in
m	Mechanical
PI	PI-Controller
PV	Photovoltaic
out	Outlet
rec	Receiver
ref	Refrigerant
scroll	Scroll compressor
swash	Swash-plate compressor
th	thermal

Abbreviation	Meaning
AC	Alternating current
CC	Compression chiller
COP	Coefficient of performance
DAQ	Data acquisition
HIL	Hardware in the loop
HP	Heat pump
PV	Photovoltaic
VFD	Variable frequency drive

8. References

American Society of Heating, Refrigerating and Air-Conditioning Engineers, Inc., 2015. ASHRAE Handbook - Heating, Ventilation, and Air-Conditioning Systems and Equipment (SI Edition). Knovel.

Bell, I.H., Wronski, J., Quoilin, S., Lemort, V., 2014. Pure and pseudo-pure fluid thermophysical property evaluation and the open-source thermophysical property library CoolProp. Ind. Eng. Chem. Res. 53, 2498–2508. https://doi.org/10.1021/ie4033999

Fischer, D., Bernhardt, J., Madani, H., Wittwer, C., 2017. Comparison of control approaches for variable speed air source heat pumps considering time variable electricity prices and PV. Appl. Energy 204, 93–105. https://doi.org/10.1016/j.apenergy.2017.06.110

Jordan, U., Vajen, K., 2017. DHWcalc Werkzeug zur Generierung von Trinkwasser-Zapfprofilen aus statistischer Basis. Universität Marburg, Marburg.

Lazzarin, R.M., Noro, M., 2018. Past, present, future of solar cooling: Technical and economical considerations. Sol. Energy. https://doi.org/10.1016/j.solener.2017.12.055

Li, H., Jeong, S.-K., You, S.-S., 2009. Feedforward control of capacity and superheat for a variable speed refrigeration system. Appl. Therm. Eng. 29, 1067–1074. https://doi.org/10.1016/j.applthermaleng.2008.05.022

Lin, Z., Wang, J., Howe, D., 2011. A Learning Feed-Forward Current Controller for Linear Reciprocating Vapor Compressors. IEEE Trans. Ind. Electron. 58, 3383–3390. https://doi.org/10.1109/TIE.2010.2089948

Luthander, R., Widén, J., Nilsson, D., Palm, J., 2015. Photovoltaic self-consumption in buildings: A review. Appl. Energy 142, 80–94. https://doi.org/10.1016/j.apenergy.2014.12.028

Poort, M.J., Bullard, C.W., 2006. Applications and control of air conditioning systems using rapid cycling to modulate capacity. Int. J. Refrig. 29, 683–691. https://doi.org/10.1016/j.ijrefrig.2005.12.007

Poppi, S., Sommerfeldt, N., Bales, C., Madani, H., Lundqvist, P., 2018. Techno-economic review of solar heat pump systems for residential heating applications. Renew. Sustain. Energy Rev. 81, 22–32.

https://doi.org/10.1016/j.rser.2017.07.041

Seborg, D.E., Mellichamp, D.A., Edgar, T.F., III, F.J.D., 2010. Process dynamics and control. John Wiley & Sons.

Sichilalu, S., Mathaba, T., Xia, X., 2017. Optimal control of a wind–PV-hybrid powered heat pump water heater. Appl. Energy, Clean, Efficient and Affordable Energy for a Sustainable Future 185, 1173–1184. https://doi.org/10.1016/j.apenergy.2015.10.072

Spinnler, M., Hörth, L., Böing, F., Wolf, S., Sattelmayer, T., 2014. Novel heat pump system for highly transient PV operation, in: 29th European Photovoltaic Solar Energy Conference and Exhibition. pp. 3562–3567.

Stulgies, N., Gräber, M., Tegethoff, W., Försterling, S., 2009. Evaluation of different compressor control concepts for a swash plate compressor, in 7th Modelica Conference, Como, Italy. pp. 299–303. https://doi.org/10.3384/ecp09430035

Thygesen, R., Karlsson, B., 2016. Simulation of a proposed novel weather forecast control for ground source heat pumps as a mean to evaluate the feasibility of forecast controls' influence on the photovoltaic electricity self-consumption. Appl. Energy 164, 579–589. https://doi.org/10.1016/j.apenergy.2015.12.013

Tian, C., Liao, Y., Li, X., 2006. A mathematical model of variable displacement swash plate compressor for automotive air conditioning system. Int. J. Refrig. 29, 270–280. https://doi.org/10.1016/j.ijrefrig.2005.05.002

Tjaden, T., Krien, U., Breyer, C., 2013. Simulation und techno-ökonomischer Vergleich von solarthermischen Heizungskonzepten und Photovoltaik-Wärmepumpen-Kombinationen im Wohnungssektor, in: 23. Symposium Thermische Solarenergie. Bad Staffelstein.

Tjaden, T.; Bergner, J.; Weniger, J.; Quaschning, V., 2015. Repräsentative elektrische Lastprofile für Einfamilienhäuser in Deutschland auf 1-sekündiger Datenbasis, Datensatz, Hochschule für Technik und Wirtschaft HTW Berlin

Wang, S.K., 2000. Handbook of air conditioning and refrigeration, 2nd ed. McGraw-Hill, New York.

9. Appendix: Test Rig Components and Measurement Equipment

Table 1: Main components of the test rig

Component	**Manufacturer / Type**	**Specifications**
Swash-plate compressor	Denso 6SEU14 / Denso 7SEU17	140 cm³ / 170 cm³ disp. vol., open casing
Scroll compressor	Emerson Copeland ZH21KW-TFD	45 cm³ disp. volume, hermetic casing
Condenser	SWEP B8THx30/1P-SC-M	Flat plate heat exchanger; Surface 0.63 m²
Evaporator		
Expansion valve	Danfoss ETS 6-14	
Superheat controller	Danfoss EKD 316	
Receiver	Klimal FM 1.6	Volume 1.6 l
AC-motor for swash-plate comp.	Dema EM 3000 STE	Max. power: 3000 W
Variable frequency drive	Danfoss VLT 3505 HV AC	Max. power 3000 W, max. frequency 80 Hz
Refrigerant	R134a	

Table 2: Measurement Equipment

Component	**Manufacturer / Type**	**Measurement Range**	**Accuracy**	**Sample Time / s**
Temperature sensors	PT1000 elements	-200 – 600 °C	+/- 0.15 K	1.13
Pressure transducers	ALCO PT5-30M	1 - 31 bar		0.25
Volume flow sensor	Kobold-Messring DTK 1210	0.05 – 0.6 l/min	+/- 2 % (FS)	0.19
Torque and rotational speed sensor	Kistler 4520A050	0 – 50 Nm; 0 – 10 000 rpm	+/- 0.5 % (FS)	0.19